

Ectopic lymphoid structures function as microniches for tumor progenitor cells in hepatocellular carcinoma

Shlomi Finkin^{1,2}, Detian Yuan³, Ilan Stein^{1,2}, Koji Taniguchi⁴, Achim Weber⁵, Kristian Unger⁶, Jeffrey L Browning⁷, Nicolas Goossens^{8,9}, Shigeki Nakagawa⁸, Ganesh Gunasekaran¹⁰, Myron E Schwartz¹⁰, Masahiro Kobayashi¹¹, Hiromitsu Kumada¹¹, Michael Berger¹, Orit Pappo², Klaus Rajewsky¹², Yujin Hoshida⁸, Michael Karin⁴, Mathias Heikenwalder^{3,13}, Yinon Ben-Neriah¹ & Eli Pikarsky^{1,2}

Ectopic lymphoid-like structures (ELSs) are often observed in cancer, yet their function is obscure. Although ELSs signify good prognosis in certain malignancies, we found that hepatic ELSs indicated poor prognosis for hepatocellular carcinoma (HCC). We studied an HCC mouse model that displayed abundant ELSs and found that they constituted immunopathological microniches wherein malignant hepatocyte progenitor cells appeared and thrived in a complex cellular and cytokine milieu until gaining self-sufficiency. The egress of progenitor cells and tumor formation were associated with the autocrine production of cytokines previously provided by the niche. ELSs developed via cooperation between the innate immune system and adaptive immune system, an event facilitated by activation of the transcription factor NF- κ B and abolished by depletion of T cells. Such aberrant immunological foci might represent new targets for cancer therapy.

A central feature of tissue inflammation is the interaction between resident cells and cells of the immune system. Cellular infiltration usually entails diffuse influx of cells of the immune system, which scatter throughout the inflamed tissue. However, infiltrating leukocytes often form simple lymphoid aggregates or even more complex structures that histologically resemble lymphoid organs^{1,2}. These structures direct various B cell and T cell responses, are organized in appropriate functional microarchitecture and are referred to as 'ectopic lymphoid-like structures' (ELSs). ELSs often develop at sites of chronic inflammation, where they influence the course of many diseases, including distinct autoimmune, cardiovascular, metabolic and neurodegenerative diseases². Although the presence of ELSs within inflamed tissues has been linked to both protective outcomes and deleterious outcomes in patients, the mechanisms that govern ectopic lymphoid neogenesis in human pathology remain poorly defined. In cancer, including solid tumors such as colorectal, lung, breast and skin carcinomas, the presence of tumor-associated ELSs correlates with a better prognosis^{3–6}. It is believed that ELSs may coordinate endogenous antitumor immune responses that improve patient survival^{1,5,7}. A role for ELSs in the premalignant phase of tumor growth has not been explored so far.

Hepatocellular carcinoma (HCC) is a major health problem, being the second leading cause of cancer-related deaths worldwide⁸. In most cases, human HCC is driven by chronic liver inflammation due to chronic viral hepatitis and non-alcoholic steatohepatitis^{9,10}. The formation of hepatic ELSs is a prominent pathological hallmark of chronic viral infection^{11,12}, yet a function for these immunological follicles in the pathogenesis of HCC has not been suggested or explored, to our knowledge. Here we found that ELSs were associated with a poor prognosis in human HCC. Furthermore, we generated a mouse model that displayed abundant hepatic ELSs before the appearance of frank HCC nodules, to investigate the pathophysiological relationship between ELSs and tumor development. ELSs constituted cytokine-rich microniches in which HCC progenitors thrived before gaining independence and moving out of the niches to form full-blown HCC. Interrupting ELS function abrogated the formation of HCC.

RESULTS

ELSs signify a poor prognosis in human HCC

To assess the relationship between the prevalence of hepatic ELSs and prognosis of human HCC, we quantified ELSs in the non-neoplastic

¹Department of Immunology and Cancer Research, Institute for Medical Research Israel Canada, Hebrew University-Hadassah Medical School, Jerusalem, Israel. ²Department of Pathology, Hadassah-Hebrew University Medical Center, Jerusalem, Israel. ³Institute of Virology, Technische Universität München, Helmholtz Zentrum München, Munich, Germany. ⁴Laboratory of Gene Regulation and Signal Transduction, Departments of Pharmacology and Pathology, School of Medicine, University of California, San Diego, La Jolla, California, USA. ⁵Institute of Surgical Pathology, University and University-Hospital Zurich, Zurich, Switzerland. ⁶Research Unit of Radiation Cytogenetics, Helmholtz-Zentrum München, Ingolstädter-Landstrasse, Neuherberg, Germany. ⁷Department of Microbiology, Boston University School of Medicine, Boston, Massachusetts, USA. ⁸Division of Liver Diseases, Department of Medicine, Liver Cancer Program, Tisch Cancer Institute, Icahn School of Medicine at Mount Sinai, New York, USA. ⁹Division of Gastroenterology & Hepatology Geneva University Hospital, Geneva, Switzerland. ¹⁰Recanati/Miller Transplantation Institute, Icahn School of Medicine at Mount Sinai, New York, USA. ¹¹Department of Hepatology, Toranomon Hospital, Tokyo, Japan. ¹²Max Delbrück Center for Molecular Medicine, Berlin, Germany. ¹³Division of Chronic Inflammation and Cancer, German Cancer Research Center, Heidelberg, Germany. Correspondence should be addressed to M.H. (heikenwalder@helmholtz-muenchen.de), Y.B.-N. (yinonb@ekmd.huji.ac.il) or E.P. (pelli@hadassah.org.il).

Received 20 July; accepted 7 September; published online 26 October 2015; doi:10.1038/ni.3290

liver parenchyma in a well-characterized cohort of 82 patients that had undergone resection of HCC, for whom we had obtained clinical data, histological slides and gene-expression data for the liver parenchyma¹³. We assessed the prevalence of ELSs histologically in 66 subjects (the subset with hematoxylin and eosin (H&E)-stained slides), using a published quantification scale¹⁴ (Fig. 1a and Supplementary Fig. 1a). This analysis revealed that in contrast to the relationship between ELS score and colon, breast, lung or skin cancer^{3–6}, a high histological ELS score was associated with increased risk for late recurrence and a trend toward decreased overall survival after HCC resection (Fig. 1b–d and Supplementary Fig. 1b–d).

A 12-gene signature has been shown to accurately assess the presence of ELSs in human tissues¹. Using expression data available for these patients, we found a strong correlation between the histological ELS score and the 12-gene ELS signature (Fig. 1a), which confirmed its utility for analysis of the liver and enabled us to expand our analysis to include all 82 patients with transcriptome profiles. We found that 15 of 82 patients (18%) had the ELS gene signature in their liver parenchyma (Fig. 1a), which was significantly associated with poor survival of patients with HCC after attempted curative surgical resection (Fig. 1b), as well as with an increased risk of late recurrence but not early recurrence (Fig. 1c and Supplementary Fig. 1e). Of note, multivariable analysis showed that the ELS gene signature was an independent prognostic factor from the 186-gene prognostic–HCC-risk gene signature previously identified for this cohort¹³, as well as the clinical prognostic staging system (Fig. 1d,e). Late recurrence, occurring 2 years after surgery, is considered to represent new carcinogenesis from the inflamed liver, while early recurrence,

within 2 years of surgery, results from the dissemination of primary tumor cells¹⁵. Collectively, our analysis of the clinical cohort suggested that ELSs were associated with new HCC development in chronically inflamed and fibrotic or cirrhotic human livers.

Association of ELSs with activation of transcription factor NF- κ B

The mechanisms underlying ELS formation in general and in cancer in particular are mostly obscure^{2,16}. To identify signaling pathways that might initiate or facilitate ELS development in HCC, we performed gene-set-enrichment analysis comparing gene expression in the liver parenchyma in patients with high ELS gene signatures and those with low ELS gene signatures. This analysis highlighted the interferon response and signaling via the transcription factor NF- κ B as top candidates (Supplementary Table 1). Further analysis of the correlation between activation of NF- κ B signaling and hepatic ELSs with three different published NF- κ B signatures confirmed the association for NF- κ B (Fig. 1f and Supplementary Fig. 1f). These findings suggested that activation of the I κ B kinase (IKK)–NF- κ B signaling pathway might be an important mediator of hepatic ELS generation.

Persistent activation of IKK in hepatocytes induces ELSs

We developed an animal model to assess the contribution of signaling via NF- κ B to the generation of ELS and HCC. To activate the IKK–NF- κ B signaling pathway in hepatocytes, we bred *R26Stop^{FL}Ikk2ca* mice (which express a transgene encoding a constitutively active form of IKK β fused to a Flag tag, as well as a stop cassette flanked by two *loxP* sites, inserted in the *Rosa26* (R26) locus, which serves as the promoter

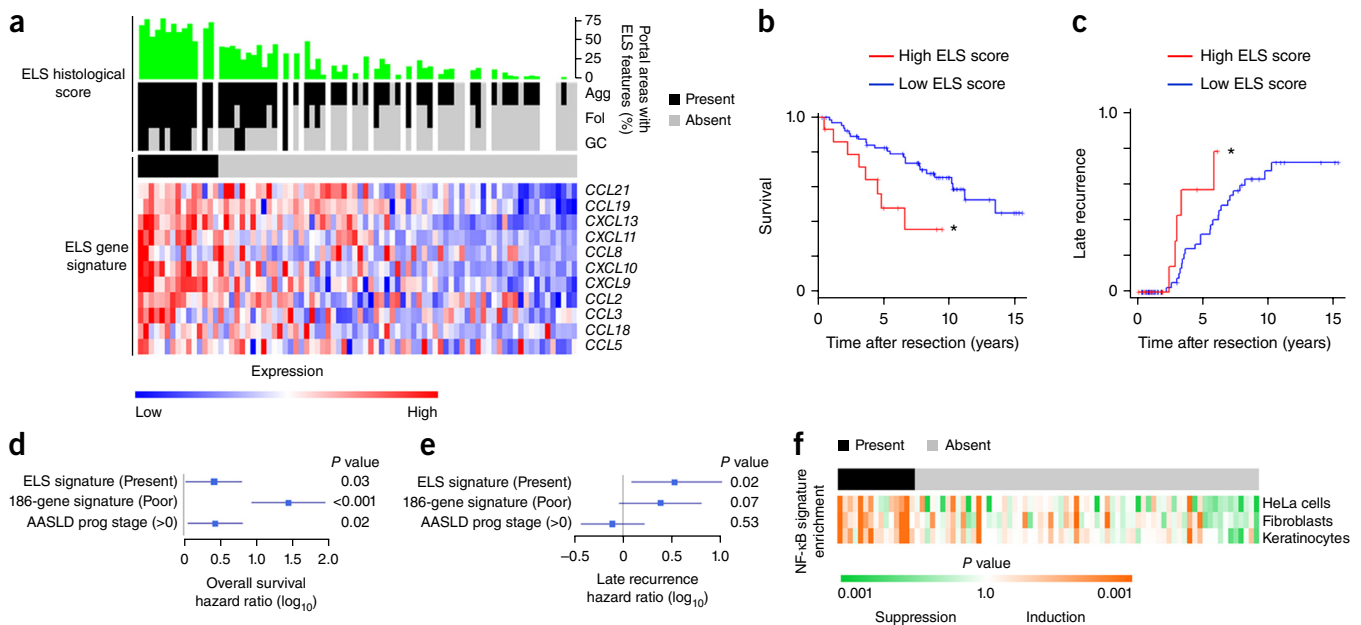
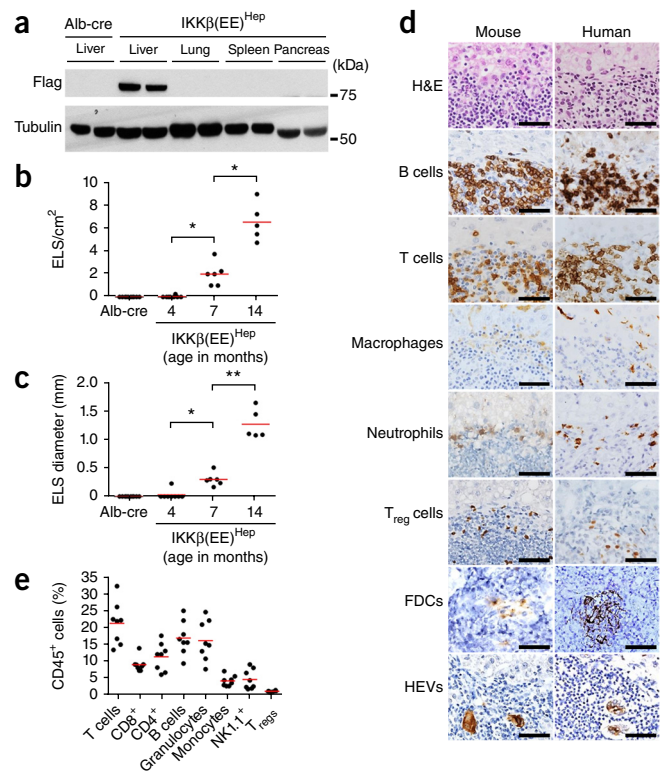


Figure 1 Hepatic ELSs signify a poor prognosis in human HCC and are associated with NF- κ B activation. **(a)** ELS histological scores (above) of samples from human donors ($n = 82$; ordered (left to right) according to ELS gene signature), presented as the proportion of portal areas with ELS features (green) (top) and type of ELS (aggregate (Agg), follicle (Fol) or germinal center (GC)), evaluated histologically as the presence or absence (key) of ELS (middle); gaps indicate lack of H&E-stained slides. Bottom, expression of each of the 12 genes in the ELS gene signature⁶; bar above, presence or absence (key) of a 'high ELS gene signature' (high expression of genes in the signature relative to the mean normalized expression of all samples; defined as described in Online Methods^{39,40}). $P < 0.001$, correlation of histological and bioinformatics ELS scores (Wilcoxon rank-sum test). **(b,c)** Survival probability (Kaplan-Meier curve; **b**) and late-recurrence probability (**c**) after resection of HCC, in patients with a high or low ELS gene signature (key) in the liver parenchyma ($n = 82$ patients (15 high; 67 low)). * $P = 0.01$ (**b**) or $P = 0.03$ (late recurrence, **c**) (log-rank test). **(d,e)** Hazard ratios of the ELS gene signature for overall survival (**d**) and late recurrence (**e**) in multivariable Cox regression modeling adjusted for 186-gene prognostic HCC risk¹³ and American Association for Study of Liver Diseases prognostic stage (AASLD prog stage)⁴¹ (horizontal bars, 95% confidence interval). **(f)** Enrichment for the NF- κ B signature in the cohort of patients in **a** (ordered (left to right) by enrichment and by presence or absence of the ELS signature (top bar; as in **a**)), determined by modulation of three experimentally defined sets of NF- κ B target genes in HeLa cells⁴², primary human fibroblasts⁴³ and keratinocytes⁴³. Data are representative of one experiment.

Figure 2 Persistent activation of IKK in the liver induces ELSs.

(a) Immunoblot analysis of Flag-tagged IKK β (EE) and tubulin (loading control) in tissues of Alb-cre (control) mice and IKK β (EE)^{Hep} mice (two per group; one mouse per lane). (b,c) Quantification of the number (b) and size (c) of ELSs in the liver of 14-month-old Alb-cre mice ($n = 10$) and 4-month-old ($n = 8$), 7-month-old ($n = 6$) or 14-month-old ($n = 5$) IKK β (EE)^{Hep} mice. * $P = 0.0002$ and ** $P = 0.00001$ (two-tailed Student's t -test). (d) H&E-stained sections (top) and immunostained sections (below) of livers from an IKK β (EE)^{Hep} mouse (left) and human patients with chronic hepatitis (right), showing ELSs. T_{reg} cells, regulatory T cells; FDCs, follicular dendritic cells; HEVs, high endothelial venules. Scale bars, 50 μ m. (e) Frequency of CD45⁺ cells among various cell subsets (horizontal axis) in ELSs microscopically isolated from the liver of IKK β (EE)^{Hep} mice ($n \geq 6$), analyzed by flow cytometry of markers indicative of those cell types. Each symbol (b,c,e) represents an individual mouse; red horizontal lines indicate the mean. Data are representative of three independent experiments (a,d) or two experiments (b,c) or are from one experiment (e).

that drives the transgene)¹⁷ with mice with transgenic expression of Cre recombinase from the promoter of the liver-specific gene encoding albumin (Alb-cre)¹⁸. The resulting IKK β (EE)^{Hep} mice expressed the constitutively active form IKK β (EE) in hepatocytes (Fig. 2a) and showed an abundance of nuclear NF- κ B and transcriptional activity of NF- κ B similar to that of Mdr2-deficient mice, a model of chronic hepatitis¹⁹, but lower than that of mice treated with tumor-necrosis factor (Supplementary Fig. 2a–d); this suggested that the activity of NF- κ B, a major activator of the innate immune system, in IKK β (EE)^{Hep} mice was similar to that in common forms of chronic hepatitis. The livers of 3-month-old IKK β (EE)^{Hep} mice lacked overt histopathology (Supplementary Fig. 2e). At 7 months, IKK β (EE)^{Hep} mice had a mild increase in liver macrophages, liver damage markers and hepatocyte proliferation compared with that of age-matched Alb-cre mice (Supplementary Fig. 2f–k). Notably, multiple ELSs were apparent in the livers of 7-month-old IKK β (EE)^{Hep} mice, and they gradually grew in both size and number, while Alb-cre mice did not develop ELSs (Fig. 2b,c). Immunohistochemical staining revealed that ELSs were composed of T lymphocytes, B lymphocytes, neutrophils (located



in the ELS periphery), natural killer cells, macrophages, regulatory T cells and follicular dendritic cells and contained high endothelial venules (Fig. 2d), which confirmed that these were true ELSs. We next analyzed ELSs present in the parenchyma of human livers with hepatitis (resected for HCC) and compared their composition of cells of the immune system with that of hepatic ELSs in IKK β (EE)^{Hep} mice. Histological analysis revealed that ELSs in IKK β (EE)^{Hep} mice were very similar to their human counterparts (Fig. 2d). Flow cytometry of single-cell suspensions of mouse ELSs confirmed the results obtained

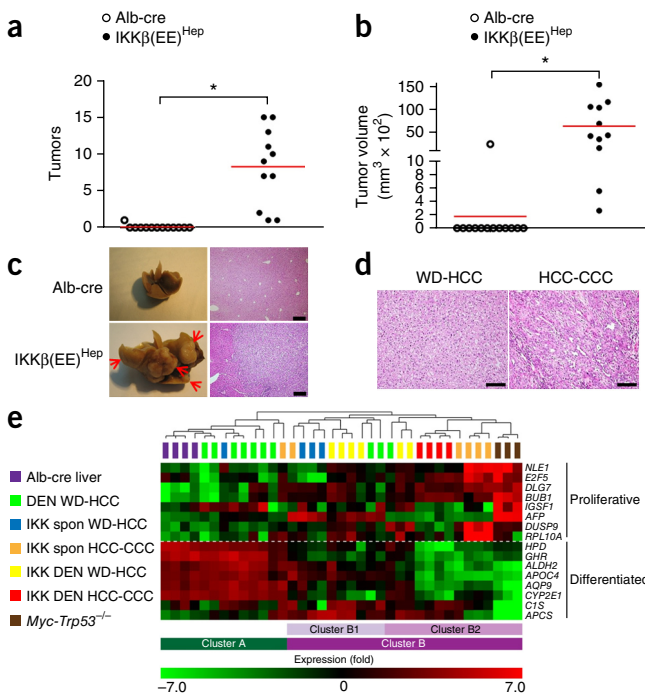
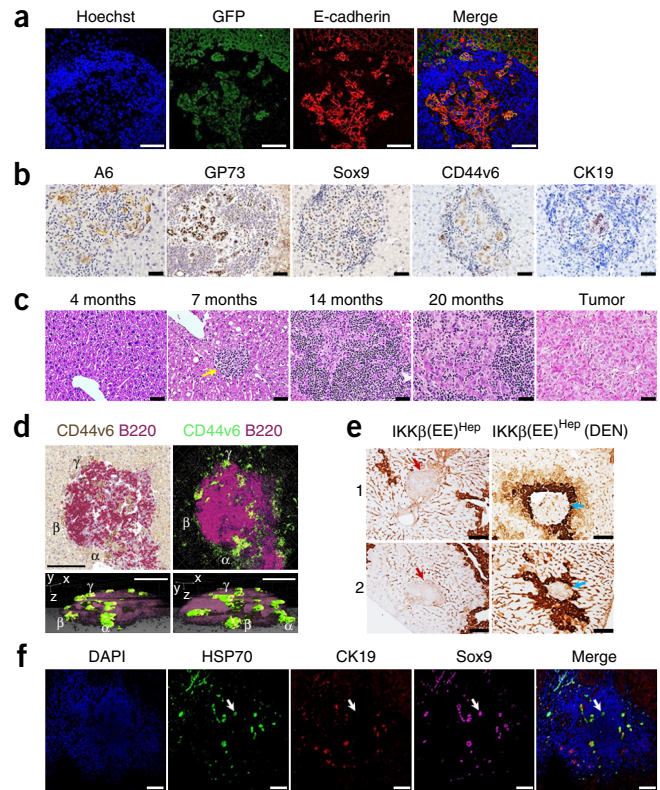


Figure 3 Persistent activation of IKK in hepatocytes induces aggressive HCC. (a,b) Quantification of tumors (≥ 0.5 cm) (a) and tumor volume (b) in the liver of 20-month-old Alb-cre mice ($n = 13$) and IKK β (EE)^{Hep} mice ($n = 11$). Each symbol represents an individual mouse; red horizontal lines indicate the mean. * $P \leq 0.0002$ (two-tailed Student's t -test). (c) Livers (left) and H&E-stained sections of liver (right) from 20-month-old Alb-cre and IKK β (EE)^{Hep} mice. Arrows indicate tumors. Scale bars, 200 μ m. (d) H&E-stained sections of WD-HCC and HCC-CCC from 20-month old IKK β (EE)^{Hep} mice. Scale bars, 100 μ m. (e) Expression of mRNA from the 16 genes of the HCC proliferation and differentiation signature²⁰ (right margin) in parenchymal liver tissue from untreated 6-month-old Alb-cre mice (Alb-cre liver) ($n = 4$), WD-HCC from 9-month-old DEN-treated Alb-cre mice (DEN WD-HCC) ($n = 10$), WD-HCC (IKK spon WD-HCC) ($n = 4$) or undifferentiated mixed HCC-CCC (IKK spon HCC-CCC) ($n = 6$) from 20-month-old IKK β (EE)^{Hep} mice, WD-HCC (IKK DEN WD-HCC) ($n = 6$) or undifferentiated mixed HCC-CCC (IKK DEN HCC-CCC) ($n = 4$) from 9-month-old DEN-treated IKK β (EE)^{Hep} mice, or HCC from *Myc-Trp53*^{-/-} mice (*Myc-Trp53*^{-/-}) ($n = 3$) (colors in key and above plot), assigned to clusters by an unsupervised algorithm; expression is relative to the average expression of all samples assessed. Top, clustering dendrogram. $P = 6.0 \times 10^{-5}$, DEN WD-HCC versus all IKK HCC (A versus B); $P = 0.001$, DEN WD-HCC versus IKK DEN (WD-HCC and HCC-CCC) (A versus B); $P = 0.04$, DEN WD-HCC versus IKK spontaneous HCC (WD-HCC and HCC-CCC) (A versus B); $P = 0.006$, DEN WD-HCC versus IKK HCC-CCC (A versus B); and $P = 0.007$, IKK WD-HCC versus IKK HCC-CCC (B1 versus B2) (two-tailed χ^2 test). Data are representative of two independent experiments (a–d) or are from one experiment (e).

Figure 4 HCC progenitor cells appear in ELSs and progressively egress. (a) Immunofluorescence staining of GFP (green) expressed from the hepatocyte-specific transgene encoding IKK β (EE) and the epithelial marker E-cadherin (red), showing the epithelial origin of HCC progenitor cells. Hoechst 33342 stain (blue) marks nuclei. Scale bars, 100 μ m. (b) Immunostaining of markers (above images) of HCC progenitor cells in ELSs of IKK β (EE)^{Hep} mice. Scale bars, 50 μ m. (c) H&E-stained sections of IKK β (EE)^{Hep} liver, showing progression from ELS to HCC (yellow arrow indicates small ELS). Scale bars, 50 μ m. (d) Three-dimensional reconstruction of an ELS from a 6-month-old DEN-treated IKK β (EE)^{Hep} mouse: top left, double-color immunostaining of CD44v6 (brown) and B220 (red); top right, color conversion of image at left (brown to green; red to purple); below, two different rotations of the reconstruction, showing CD44v6⁺ progenitor cells (green) egressing from the ELS at multiple points (α , β and γ mark the same region in all images; additional data, **Supplementary Video 1**). Scale bars 100 μ m. (e) Immunostaining of the pericentral marker glutamine synthetase in livers from 14-month-old untreated IKK β (EE)^{Hep} mice and 6-month-old DEN-treated IKK β (EE)^{Hep} mice ($n = 2$ per group (1 and 2, left margin)): arrows indicate periportal ELSs (red) and pericentral ELSs (blue); brown staining indicates pericentral zones. Scale bars, 100 μ m. (f) Confocal microscopy of ELS-containing liver sections from a human patient, stained for the HCC progenitor cell markers HSP70 (green) and Sox9 (purple) and for the bile duct marker CK19 (red), and with the DNA-binding dye DAPI (blue) to mark the nuclei; arrows indicate a group of HCC progenitor cells. Scale bars, 100 μ m. Data are representative of three independent experiments (a,b) or two experiments (c) or are from one experiment (d–f).



by immunohistochemical analysis (**Fig. 2e** and **Supplementary Fig. 2l,m**). We also observed compartmentalization of B lymphocytes and T lymphocytes, another characteristic feature of ELSs, in ELSs of IKK β (EE)^{Hep} mice and human hepatitis (**Supplementary Fig. 2n**). Furthermore, the ELS gene signature was upregulated in the liver parenchymas of IKK β (EE)^{Hep} mice compared with the expression of these genes in Alb-cre mice ($P < 0.05$ (two-tailed Student's t -test); **Supplementary Fig. 2o** and **Supplementary Table 2**). Thus, persistent activation of IKK in hepatocytes might be a key mediator of the formation of hepatic ELSs in human hepatitis.

Hepatic ELSs herald aggressive HCCs in IKK β (EE)^{Hep} mice

At 20 months of age, 100% of IKK β (EE)^{Hep} mice developed HCC, compared with 8% of Alb-cre mice (**Fig. 3a–c**). Histological analysis revealed that approximately half of IKK β (EE)^{Hep} tumors were well-differentiated HCCs (WD-HCCs); the remaining tumors were mixed cholangio-hepatocellular carcinomas (HCC-CCCs), indicated by the presence of malignant glandular structures (**Fig. 3d**). Immunostaining of the HCC markers A6 and glutamine synthetase, the proliferation marker Ki67 and matrix-associated collagen IV (whose expression is downregulated in HCC), as well as the presence of metastases to lymph nodes and lungs, confirmed that these were aggressive, malignant HCCs (**Supplementary Fig. 3a–c**). Notably, mice with a single allele encoding IKK β (EE) had a lower number and size of ELSs at 14 months (**Supplementary Fig. 3d,e**), followed by a similar lower HCC load at 20 months, than that of mice with two such alleles (**Supplementary Fig. 3f,g**); this underscored the 'NF- κ B dose-dependent' ELS phenotype and association between ELSs and HCC, respectively.

We also generated mice in which expression of the transgene encoding IKK β (EE) was driven by the promoter of the gene encoding albumin (Alb-IKK β (EE) mice). Of note, these mice also had ELSs and mild inflammation, followed by the development of HCC (**Supplementary Fig. 3h–j**), which confirmed the hepatocarcinogenic effect of constitutive expression of IKK β (EE) in hepatocytes in a distinct mouse model. Treatment of IKK β (EE)^{Hep} mice with the hepatic carcinogen diethylnitrosamine (DEN) accelerated the appearance of ELSs (which

appeared at 3 months in these conditions) and HCCs (which appeared at 9 months in these conditions), without altering their histological or molecular characteristics (**Supplementary Fig. 3k–r**).

Analysis of the expression of a 16-gene set for assessment of HCC aggressiveness²⁰ revealed that the expression pattern of HCCs from DEN-treated wild-type mice tended to cluster with that of wild-type livers (seven of ten HCCs), while the expression pattern of HCCs from IKK β (EE)^{Hep} mice clustered with that of aggressive HCCs from mice with transgenic overexpression of the oncogene *Myc* in hepatocytes together with germline deletion of the gene encoding the tumor suppressor p53 (*Myc-Trp53^{-/-}*) (eighteen of twenty HCCs) (**Fig. 3e**). The gene-expression pattern of tumors displaying the HCC-CCC morphology, which we detected only in IKK β (EE)^{Hep} mice and not in DEN-treated (control) mice, clustered with that of the more aggressive group (**Fig. 3e**). Of note, we did not detect a difference between spontaneous HCCs and DEN-induced HCCs in IKK β (EE)^{Hep} mice in their gene-expression patterns (**Fig. 3e**). Array-based comparative genomic hybridization (CGH) analysis of HCCs from DEN-treated Alb-cre mice ($n = 12$), DEN-treated IKK β (EE)^{Hep} mice ($n = 11$) and 20-month-old IKK β (EE)^{Hep} mice ($n = 13$) revealed chromosomal aberrations in all HCC samples (ArrayExpress accession code **E-MTAB-3848**), which confirmed their neoplastic nature. Mixed HCC-CCC tumors were more complex than were WD-HCCs (**Supplementary Fig. 3s**). To confirm the results of the CGH analysis reported above, we prepared digital PCR probes directed at two genes, *Rgs2* and *Gab2*, and thereby assessed the two most common genomic amplifications. This analysis revealed a 90% concordance with results of the array CGH analysis (**Supplementary Fig. 3t**). In addition, analysis of 13 additional IKK β (EE)^{Hep} HCCs revealed amplification of the *Rgs2* copy number in 38% of the HCCs tested and amplification of the *Gab2* copy number in 30% of the HCCs tested (**Supplementary Fig. 3t**). Together these data confirmed that IKK β (EE)^{Hep} mice developed aggressive HCCs with 100% penetrance.

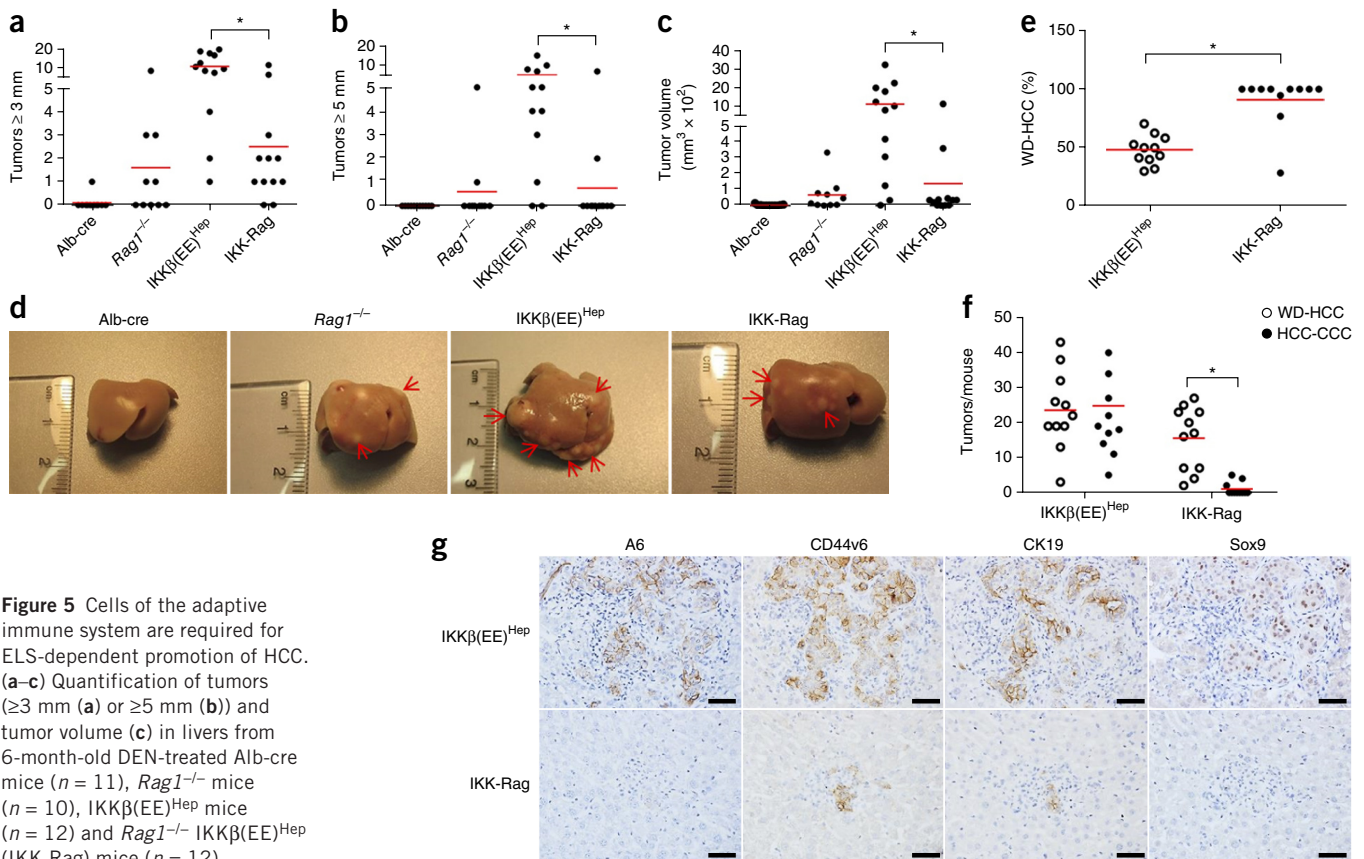


Figure 5 Cells of the adaptive immune system are required for ELS-dependent promotion of HCC. (a–c) Quantification of tumors (≥ 3 mm (a) or ≥ 5 mm (b)) and tumor volume (c) in livers from 6-month-old DEN-treated Alb-cre mice ($n = 11$), $Rag1^{-/-}$ mice ($n = 10$), $IKK\beta(EE)^{Hep}$ mice ($n = 12$) and $Rag1^{-/-} IKK\beta(EE)^{Hep}$ (IKK-Rag) mice ($n = 12$).

* $P \leq 0.006$ (two-tailed Student's t -test). (d) Images of livers from mice as in a; red arrows indicate tumors. (e, f) Proportion of WD-HCC among all tumors in each mouse (e) and quantification of tumors classified as WD-HCC or HCC-CCC (f) in DEN-treated $IKK\beta(EE)^{Hep}$ mice and $Rag1^{-/-} IKK\beta(EE)^{Hep}$ mice ($n = 11$ per group). * $P \leq 0.00004$ (two-tailed Student's t -test). (g) Immunostaining of the HCC progenitor cell markers A6, CD44v6, CK19 and Sox9 in livers from 6-month-old DEN-treated $IKK\beta(EE)^{Hep}$ mice and $Rag1^{-/-} IKK\beta(EE)^{Hep}$ mice. Scale bars, 50 μm . Each symbol (a–c, e, f) represents an individual mouse; small red horizontal lines indicate the mean. Data are from one experiment.

HCC progenitor cells first appear inside ELSs and later egress

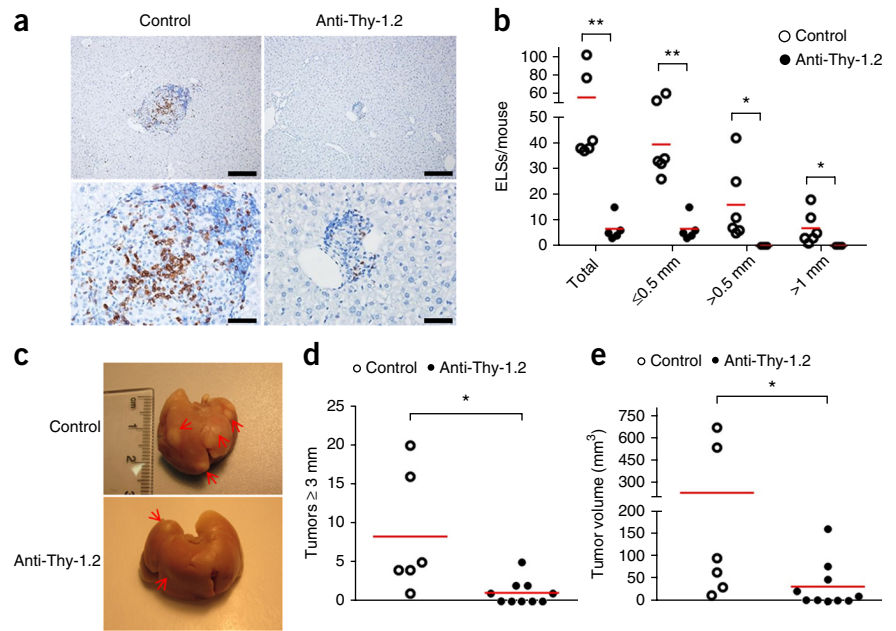
Careful histological analysis revealed that the earliest malignant hepatocytes (noted at 3 months in DEN-treated mice and at 7 months in untreated $IKK\beta(EE)^{Hep}$ mice) appeared first within newly formed ELSs (Fig. 4a–c). These malignant hepatocytes were doubly positive for green fluorescent protein (GFP) (expressed from the hepatocyte-specific transgene encoding $IKK\beta(EE)$) and E-cadherin (Fig. 4a), which confirmed their hepatocyte origin and epithelial phenotype, and they expressed multiple markers of HCC progenitor cells, including A6, GP73 (GOLPH2), Sox9, CD44v6 (ref. 21) and CK19 (Fig. 4b). At these earliest time points, HCC progenitor cells were present mainly in ELSs and not elsewhere in the liver parenchyma (Supplementary Fig. 4a–c). GFP expression proved that these cells were derived from hepatocytes expressing the Alb-cre transgene (Supplementary Fig. 4d). These small clusters gradually grew, initially within ELSs, and later migrated out to form visible tumors (Fig. 4c and Supplementary Fig. 4e). We consistently noted this histological sequence (small groups of cells first appearing within ELSs, followed with gradual coalescence of groups of cells within the follicle boundary, which finally grew out into full-blown HCCs) in all $IKK\beta(EE)^{Hep}$ mice of appropriate age in both spontaneous (untreated) groups and DEN-treated groups (Supplementary Fig. 4f, g). To unequivocally prove the neoplastic nature of the epithelial cells that grew within the ELSs, we used laser-capture micro-dissection to collect enriched populations of these cells. Indeed, three of eleven lesions had amplification of *Rgs2*,

and one of eleven lesions had amplification of *Gab2* (Supplementary Fig. 4h), which confirmed the neoplastic nature of these lesions and provided a genetic link between the malignant cells that were thriving within the ELSs and the HCCs of $IKK\beta(EE)^{Hep}$ mice.

Of note, several months after the first appearance of ELSs, we consistently observed clusters of malignant hepatocytes budding from the ELSs (Supplementary Fig. 4i). These clusters were either in continuity with or slightly separated from the intra-ELS malignant cells (Supplementary Fig. 4i). To better visualize the egress of clusters of malignant cells, we immunostained serial sections with antibody to CD44v6 (a marker for HCC progenitor cells²¹) and antibody to the B cell-associated marker B220 and generated three-dimensional reconstructions of ELSs. The result showed clusters of malignant cells budding out of ELSs (Fig. 4d and Supplementary Video 1).

Although the transgene encoding $IKK\beta(EE)$ was expressed throughout the parenchyma, ELSs were focal (data not shown), which suggested that additional factors triggered the formation of the ELSs. Our finding that the appearance of ELSs was accelerated by the administration of DEN (Supplementary Fig. 3l, m) suggested that tissue damage might be of relevance, either by focal enhancement of activation of NF- κ B in hepatocytes or by triggering of another cooperating pro-inflammatory pathway. To investigate this, we analyzed the microanatomical localization of ELSs relative to various liver zones. DEN is converted to its active metabolite in pericentral hepatocytes. Thus, if genotoxic stress were directly involved in

Figure 6 Anti-Thy-1.2 immunoablative treatment during ELS development attenuates liver tumorigenesis. **(a)** Immunostaining of CD3 in livers from 6-month-old DEN-treated IKK β (EE)^{Hep} mice given injection of control antibody or anti-Thy-1.2 ($n \geq 6$ mice per group). Scale bars, 200 μ m (top) or 50 μ m (bottom). **(b)** Quantification of total ELSs (far left) and ELSs of various sizes (horizontal axis) in sections from the entire liver of mice treated with control antibody ($n = 6$) or anti-Thy-1.2 ($n = 5$). * $P \leq 0.04$ and ** $P \leq 0.003$ (two-tailed Student's t -test). **(c)** Images of livers from 6-month-old DEN-treated IKK β (EE)^{Hep} mice given injection of control antibody ($n = 6$ mice) or anti-Thy-1.2 ($n = 10$ mice); arrows indicate tumors. **(d,e)** Quantification of tumors (≥ 3 mm) **(d)** and tumor volume **(e)** in livers of 6-month-old DEN-treated IKK β (EE)^{Hep} mice treated with control antibody ($n = 6$ mice) or anti-Thy-1.2 ($n = 10$ mice). * $P \leq 0.04$ (two-tailed Student's t -test). Each symbol **(b,d,e)** represents an individual mouse; red horizontal lines indicate the mean. Data are from one experiment.



the formation of ELSs, the ELSs would be localized to pericentral regions. Immunostaining of glutamine synthetase (a marker of pericentral hepatocytes) revealed that ELSs were evenly distributed in the three liver zones in untreated IKK β (EE)^{Hep} mice; however, in DEN-treated IKK β (EE)^{Hep} mice, ELSs were limited almost entirely to the pericentral zone (Fig. 4e and Supplementary Fig. 4j), which suggested a causal relationship between genotoxic stress and ELS formation.

To investigate whether HCC progenitor cells were also present in ELSs of human patients, we analyzed liver parenchyma from human livers resected for HCC. Triple-immunofluorescence with antibodies to the human HCC markers HSP70 and SOX9 together with antibody to CK19 (which marks reactive ductular cells) revealed the presence of cells with HCC progenitor features within the human ELSs (Fig. 4f), which attested to a common ELS-related pathogenic mechanism in human HCC and the mouse model.

Depletion of ELSs attenuates mouse HCC

The adaptive immune system is commonly considered a defense mechanism against cancer progression. Accordingly, human HCCs with substantial lymphocytic infiltration have a better prognosis²², and *Rag1*^{-/-} mice, which lack an adaptive immune system, have more HCCs after treatment with DEN²³. However, despite its defense function, activation of the immune system can result in various pathologies, including cancer^{24,25}.

To assess the function of ELSs in hepatocarcinogenesis, we bred IKK β (EE)^{Hep} mice with *Rag1*^{-/-} mice, which completely lack B cells and T cells. Consistent with a published report²³, there was a slightly greater number of HCCs in DEN-treated *Rag1*^{-/-} mice than in DEN-treated Alb-cre mice (Fig. 5a–d). As expected, deletion of *Rag1* in IKK β (EE)^{Hep} mice resulted in complete elimination of ELSs (data not shown). However, in contrast to its pro-tumorigenic effect in *Rag1*^{-/-} mice, loss of the adaptive immune system in *Rag1*^{-/-} IKK β (EE)^{Hep} mice substantially attenuated hepatocarcinogenesis; most if not all of the pro-tumorigenic effect of the transgene encoding IKK β (EE) was lost in the absence of *Rag1* (Fig. 5a–d). The tumors that did develop in *Rag1*^{-/-} IKK β (EE)^{Hep} mice were exclusively typical WD-HCCs and were negative for most markers of HCC progenitor cells (Fig. 5e–g).

As expected, HCC progenitor cells in IKK β (EE)^{Hep} liver were within ELSs; however, the rare ones occasionally seen in IKK β (EE)^{Hep} *Rag1*^{-/-} mice were in the parenchyma (Fig. 5g). Comparison of the proliferation, apoptosis and accumulation of the NF- κ B subunit RelA (p65) in the nucleus of the HCCs of *Rag1*^{-/-} IKK β (EE)^{Hep} mice and in the well-differentiated HCCs of IKK β (EE)^{Hep} mice did not reveal differences (Supplementary Fig. 5a–f), which challenged the possibility of a cell-autonomous effect of *Rag1* deficiency on HCC growth. Together these data suggested that the generation of the focal immunological microniche was dependent on a functional adaptive immune system and that the immunological microniche promoted HCC.

To determine whether ablation of ELS function after the induction of tumors by DEN could still affect HCC formation in IKK β (EE)^{Hep} mice, we administered antibody to the alloantigen Thy-1.2 (anti-Thy-1.2), to ablate T cells (and potentially also innate lymphoid cells and natural killer cells, which are also reported to respond to such treatment), to mice between 18 and 30 weeks of age; control mice received an isotype-matched control antibody (Supplementary Fig. 6a). Immunostaining of the invariant signaling protein CD3 in livers confirmed almost complete ablation of T cells (Fig. 6a). Indeed, treatment with anti-Thy-1.2 restricted ELS development (Fig. 6b), and markedly reduced the multiplicity and burden of HCCs in IKK β (EE)^{Hep} mice (Fig. 6c–e and Supplementary Fig. 6b–d). Thus, the adaptive immune system had a strong pro-tumorigenic effect in IKK β (EE)^{Hep} mice, which took place after acquisition of the initiating tumor mutations.

High expression of growth-promoting cytokines in ELSs

We hypothesized that cytokines secreted by cells of the adaptive immune system, possibly present at high concentrations within ELSs, might underlie their tumor-promoting effects. To identify pro-tumorigenic signals operative within ELSs, we measured the expression of various cytokines in liver parenchyma, ELSs and HCCs from IKK β (EE)^{Hep} mice and humans with chronic viral hepatitis. Among others, members of the lymphotoxin family, in particular LT β and LIGHT (TNFSF14), and their downstream effectors, the chemokines CCL17 and CCL20, were prominently overexpressed in human and mouse samples, along with signs of lymphotoxin-driven non-canonical

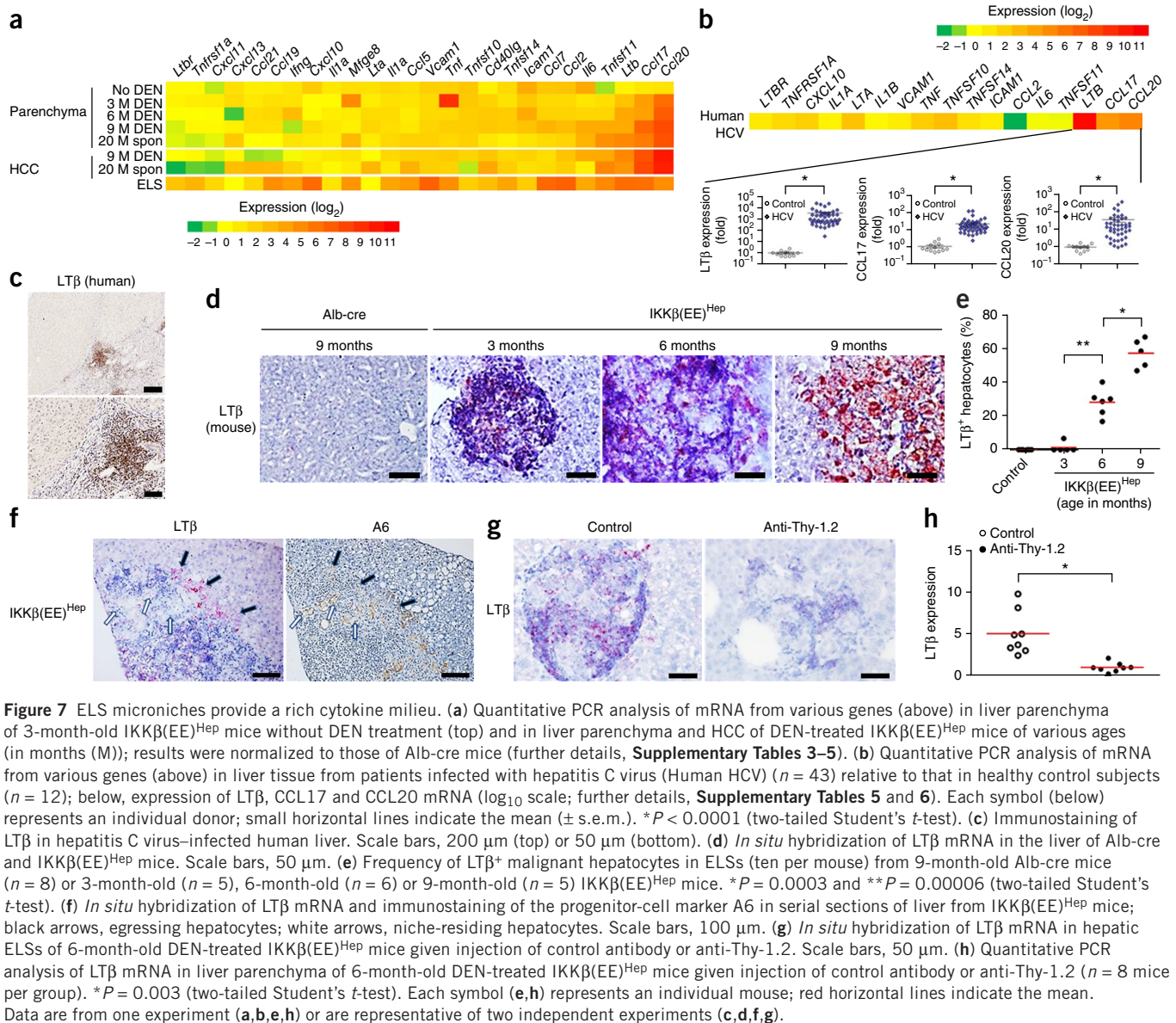
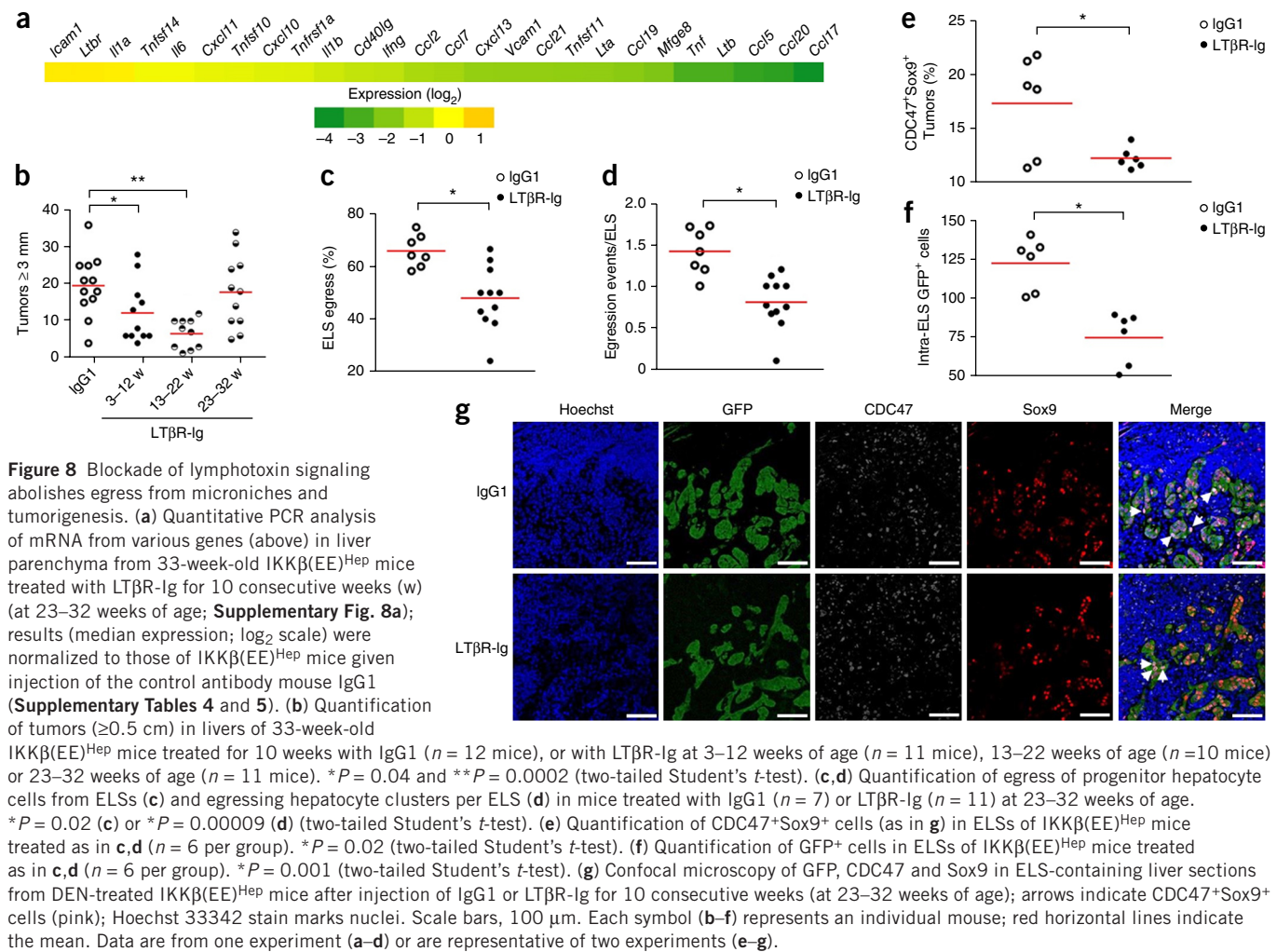


Figure 7 ELS microniches provide a rich cytokine milieu. **(a)** Quantitative PCR analysis of mRNA from various genes (above) in liver parenchyma of 3-month-old IKKβ(EE)^{Hep} mice without DEN treatment (top) and in liver parenchyma and HCC of DEN-treated IKKβ(EE)^{Hep} mice of various ages (in months (M)); results were normalized to those of Alb-cre mice (further details, **Supplementary Tables 3–5**). **(b)** Quantitative PCR analysis of mRNA from various genes (above) in liver tissue from patients infected with hepatitis C virus (Human HCV) ($n = 43$) relative to that in healthy control subjects ($n = 12$); below, expression of LTβ, CCL17 and CCL20 mRNA (log₁₀ scale; further details, **Supplementary Tables 5 and 6**). Each symbol (below) represents an individual donor; small horizontal lines indicate the mean (\pm s.e.m.). $*P < 0.0001$ (two-tailed Student's *t*-test). **(c)** Immunostaining of LTβ in hepatitis C virus-infected human liver. Scale bars, 200 μm (top) or 50 μm (bottom). **(d)** *In situ* hybridization of LTβ mRNA in the liver of Alb-cre and IKKβ(EE)^{Hep} mice. Scale bars, 50 μm. **(e)** Frequency of LTβ⁺ malignant hepatocytes in ELSs (ten per mouse) from 9-month-old Alb-cre mice ($n = 8$) or 3-month-old ($n = 5$), 6-month-old ($n = 6$) or 9-month-old ($n = 5$) IKKβ(EE)^{Hep} mice. $*P = 0.0003$ and $**P = 0.00006$ (two-tailed Student's *t*-test). **(f)** *In situ* hybridization of LTβ mRNA and immunostaining of the progenitor-cell marker A6 in serial sections of liver from IKKβ(EE)^{Hep} mice; black arrows, egressing hepatocytes; white arrows, niche-residing hepatocytes. Scale bars, 100 μm. **(g)** *In situ* hybridization of LTβ mRNA in hepatic ELSs of 6-month-old DEN-treated IKKβ(EE)^{Hep} mice given injection of control antibody or anti-Thy-1.2. Scale bars, 50 μm. **(h)** Quantitative PCR analysis of LTβ mRNA in liver parenchyma of 6-month-old DEN-treated IKKβ(EE)^{Hep} mice given injection of control antibody or anti-Thy-1.2 ($n = 8$ mice per group). $*P = 0.003$ (two-tailed Student's *t*-test). Each symbol (**e,h**) represents an individual mouse; red horizontal lines indicate the mean. Data are from one experiment (**a,b,e,h**) or are representative of two independent experiments (**c,d,f,g**).

activation of the NF-κB pathway (**Fig. 7a,b** and **Supplementary Fig. 7a–d**). LTβ was also expressed in ELSs of patients with chronic hepatitis (**Fig. 7b,c**). Moreover, we noted a correlation between the expression of CCL17 and CCL20 mRNA and that of LTβ in samples from both mice and humans ($P < 0.05$ (Spearman and Pearson correlation tests, respectively); **Supplementary Fig. 7e–h**). This suggested that activation of the receptor for LTβ (LTβR) by LTα, LTβ and/or LIGHT might have a key role in ELS assembly and pro-tumorigenic processes^{26–29}. LTβR is reported to be expressed on hepatocytes, whereas LTα and LTβ are normally expressed in lymphocytes³⁰. Indeed, mRNA *in situ* hybridization revealed that LTβ mRNA was expressed in cells of the immune system, but not epithelial cells, in small ELSs (**Fig. 7d** and **Supplementary Fig. 7i**).

To identify the specific cell types that expressed LTβ, we used flow cytometry to sort single-cell suspensions of ELSs. This analysis revealed that LTβ mRNA was expressed by both T lymphocytes and B lymphocytes but not by hepatocytes (**Supplementary Fig. 7j**). However, in advanced, large ELSs, some of the neoplastic hepatocytes also expressed LTβ, and all full-blown HCCs always expressed

LTβ mRNA, as assessed by histology (**Fig. 7d** and **Supplementary Fig. 7i**). Notably, when varying degrees of expression were present in malignant hepatocytes within an ELS, there was expression of LTβ mRNA in malignant hepatocytes at the ELS periphery, in particular within the egressing clusters (**Fig. 7e,f** and **Supplementary Fig. 7k,l**). This raised the hypothesis that cells of the immune system within the ELSs might provide paracrine lymphotoxin signals to early HCC progenitor cells, which would be later replaced by an autocrine signal, allowing the malignant hepatocytes to gain independence from the niche. This presumption might be supported by the observation that transgenic overexpression of LTα and LTβ in hepatocytes induces HCC²⁶. Notably, HCCs that developed in IKKβ(EE)^{Hep} mice after treatment with anti-Thy-1.2 and in *Rag1*^{-/-} IKKβ(EE)^{Hep} livers showed much lower expression of LTβ mRNA than that in similar mice treated with control antibody (**Fig. 7g,h** and **Supplementary Fig. 7m–p**); this suggested that exposure of tumor progenitor cells at early stages to niche-derived cytokines rendered them 'addicted' to these cytokines and favored the acquisition of autocrine abilities for production of the same cytokines.



To test that hypothesis, we blocked lymphotoxin cytokines through the use of soluble LT β R fused to mouse immunoglobulin Fc fragment (LT β R-Ig)²⁶. Furthermore, to determine the time point at which this blockade was most effective, we subjected IKK β (EE)^{Hep} mice to the following three treatment regimens: at 3–12 weeks of age (early), when LT β was expressed by cells of the immune system in ELSs; at 13–22 weeks of age (intermediate), when LT β was expressed by both cells of the immune system and malignant cells in ELSs; and 23–32 weeks of age (late), during which period LT β had expression similar to that in the intermediate period, yet HCCs were more developed (**Supplementary Fig. 8a,b**). Measurement of the expression of various cytokine-encoding genes in liver parenchyma showed lower expression of many genes encoding pro-inflammatory cytokines and lymphotoxin-mediated cytokines in LT β R-Ig-treated IKK β (EE)^{Hep} mice than in IKK β (EE)^{Hep} mice treated with the control antibody mouse immunoglobulin G1 (IgG1) (**Fig. 8a**). Of note, the blockade of lymphotoxin signaling was associated with reduced activation of NF- κ B in ELS-residing malignant hepatocytes (**Supplementary Fig. 8c,d**), which suggested that lymphotoxin signaling enhanced the low level of NF- κ B activation induced by the transgene encoding IKK β (EE). Notably, treatment with LT β R-Ig in the early and intermediate periods substantially diminished the HCC burden (**Fig. 8b** and **Supplementary Fig. 8e,f**). In contrast, inhibition of LT β R signaling at the late period resulted in a smaller, non-significant effect on HCC number and tumor volume

(**Fig. 8b** and **Supplementary Fig. 8e,f**). As inhibition of lymphotoxin proved ineffective in reducing tumorigenesis beyond 23 weeks of age, we hypothesized that the main inhibitory effect of lymphotoxin blockade might have been in ELSs, in which lymphotoxin is provided mainly by the lymphocytes, rather than in an autocrine manner by niche-external tumor cells. Indeed, histological inspection of early tumorigenesis stages in the late-treatment group revealed a substantial reduction in the number of intra-ELS HCC progenitor cells and in both the multiplicity and size of clusters of egressing cells (**Fig. 8c,d** and **Supplementary Fig. 8g**). This was associated with reduced proliferation of HCC progenitor cells (CDC47⁺Sox9⁺) in ELSs upon treatment (**Fig. 8e–g**), which might have accounted for the lower number of ELS-egressing atypical hepatocytes (**Fig. 8c,d**). It thus appeared that paracrine lymphotoxin stimulation within ELSs was a critical step in HCC development, amenable to anti-tumor intervention.

DISCUSSION

Our study has revealed a liver tumorigenesis program whereby specialized ELSs, associated with chronic NF- κ B activation, fostered atypical hepatocytes that eventually acquired malignant properties. Notably, our study indicated that ELSs, which are commonly present in human livers with HCC, promoted tumor development, rather than counteracting it, as has been demonstrated for several tumor types^{3–7}. This indicates contrasting roles for ELSs in cancer that might

be related to the different cancer types or might reflect alternative phenotypes of ELSs. Shortly after ELS expansion and the egress of tumor progenitor cells, we observed distinct tumors with similar chromosomal aberrations, which indicated that the tumors originated from ELS-nested atypical hepatocytes. The pro-tumorigenic effect of ELSs required a competent adaptive immune system that provided lymphocyte-derived cytokines and supported HCC progenitors until they were ready to egress from their niches. Related hepatic ELSs are commonly found in patients with chronic hepatitis who are at risk of developing HCC; hence, these ELSs might constitute a microniche for the population of expanding HCC progenitor cells that support cancer development. Similar to results obtained for our mouse models, these human follicles might form due to constitutive activation of IKK by chronic infection with hepatitis virus (for example, hepatitis B virus³¹ or hepatitis C virus^{32,33}). We may have therefore identified a critical window of immunological-inflammatory action in tumor development: the intra-niche growth of early tumor progenitor cells. The immunological microniche environment seemed to provide tumor progenitor cells with crucial survival and growth factors. Accordingly, preventing niche assembly or interfering with niche function significantly reduced the HCC load in IKK β (EE)^{Hep} mice. ELSs are unique micro-anatomical structures that are commonly observed in disease states, including cancer². Specifically in the liver, ELSs are associated with chronic hepatitis^{11,12,34}. Our IKK β (EE)^{Hep} model has provided functional information about ELSs, showing that they furnished a unique microenvironment that supported growth of tumor progenitor cells. This was confirmed by our studies of humans that showed a higher probability of late recurrence and death after HCC resection in patients with a large number of hepatic ELSs. Of note, late recurrence, occurring 2 years after surgery, is considered to represent *de novo* carcinogenesis¹⁵.

Although our experiments with *Rag1*^{-/-} mice confirmed published studies showing that certain cells of the adaptive immune system can serve an anti-tumor role in hepatocarcinogenesis (i.e., in the absence of IKK-induced ELS formation), they revealed the substantial pro-tumorigenic potential of cells of the adaptive immune system in specific structures such as the ELS. An obvious difference between the pro-tumorigenic states and anti-tumorigenic states is formation of highly structured microanatomical structures composed of hundreds of cells of the immune system, in which the dominant effect is pro-tumorigenic. It is becoming clear that in lymphatic organs, three-dimensional structures are key for shaping intercellular communication and cooperation among various types of cells of the immune system, frequently involving physical cell-cell interactions that are meticulously orchestrated to generate multiple effector mechanisms and bestow different phenotypes on the interacting cells³⁵. Thus, the unique structure of the ELS, as well as structural and composition changes over time, might explain how the adaptive immune system turns from anti-tumorigenic to pro-tumorigenic. The compact structure of the ELS, which groups together large numbers of cells of the immune system, probably suffices to generate a niche containing high concentrations of cytokines and growth factors derived from cells of the immune system that provide a tumor-promoting environment.

The formation of ELSs is thought to depend on innate lymphoid tissue-inducer cells that are recruited to extranodal sites by chemoattracting cytokines². The association between the activation of NF- κ B and number of ELSs in human livers and the 100% prevalence of ELSs in IKK β (EE)^{Hep} livers would suggest that activation of hepatocyte NF- κ B (known to occur in chronic hepatitis of diverse etiologies) has a role in ELS formation in the liver, which would link instigation of epithelial innate immunity and focal activation of adaptive immunity³⁶.

Although NF- κ B was activated throughout the liver of IKK β (EE)^{Hep} mice, ELSs were focal, which would suggest that additional cues are needed. The finding that ELS formation was significantly accelerated by DEN would suggest that genotoxic stress might have a role in ELS formation. In support of that was the difference in the distribution of ELSs. In untreated IKK β (EE)^{Hep} mice, ELSs were evenly distributed between liver zones, whereas in DEN-treated mice, the ELSs were located mainly in the pericentral zone, where DEN is converted from a pro-carcinogen to a carcinogen that can attack DNA³⁷. This joint activation of the NF- κ B and DNA damage-response pathways might generate a threshold level of cytokines sufficient to elicit the formation of ELSs. Of note, although a published report has suggested that a persistently active transgene encoding IKK expressed in hepatocytes does not lead to HCC induction³⁸, it is plausible that either the expression level was not sufficiently high or that the follow-up time was not long enough. Indeed, we found that mice with a single allele encoding IKK β (EE) showed diminished tumor load compared with that of mice with two such alleles, which demonstrated that the level of expression of the transgene was important. Furthermore, we noted HCC development in two different strains of mice with transgenic expression of IKK, kept in different facilities.

The egress of tumor cells from the niche in which they first grew was a notable phenomenon we observed in IKK β (EE)^{Hep} mice. Seeds of cancer might germinate in an appropriate microenvironment, yet are capable of leaving the nursing niche and form full-blown malignant tumors only upon acquiring new capabilities. We speculate that the acquisition of niche independence is a hallmark prerequisite of solid tumors initiated within a supportive niche. One specific mechanism we detected in IKK β (EE)^{Hep} mice was the acquisition of autocrine lymphotoxin expression, but others probably also took place. Tumor progenitor cells have been shown to respond to interleukin 6 from resident tissue macrophages, but later acquired autocrine signaling via interleukin 6 that promoted malignant progression²¹. Identifying additional examples of immune system-dependent tumor microniches, as well as their support of tumor progenitor cells and egress mechanisms thereof, might guide effective ways for interfering with these processes for therapeutic purposes.

METHODS

Methods and any associated references are available in the [online version of the paper](#).

Accession codes. ArrayExpress: CGH analyses [E-MTAB-3848](#).

Note: Any Supplementary Information and Source Data files are available in the online version of the paper.

ACKNOWLEDGMENTS

We thank K. Kohno (Nara Institute of Science and Technology) for plasmids pBstN and p2335A-1; M.-A. Buendia (Institut Pasteur, France) for *Myc-Trp53*^{-/-} liver tumors; V. Factor and S. Thorgeirsson (US National Institutes of Health) for anti-A6; and E. Cinnamon, M.-A. Buendia, K. Kohno, M. Ringelhan, R. Hillermann, D. Kull, I. Gat-Viks, Y. Steuerman, S. Itzkovitz and K. Bahar-Halpern for help and advice. Supported by the Dr. Miriam and Sheldon G. Adelson Medical Research Foundation (E.P. and Y.B.-N.), the European Research Council (LIVERMICROENV to E.P.; PICH0 to Y.B.-N.; and LiverCancerMechanism to M.H.), the Israel Science Foundation (E.P., Y.B.-N., I.S. and O.P.), the Israel Cancer Research Fund (Y.B.-N.), the Helmholtz alliance "preclinical comprehensive cancer center" Graduiertenkolleg (GRK482 to M.H.), Krebsliga Schweiz (Oncosuisse) (A.W.), Promedica Stiftung (A.W.), the US National Institutes of Health (CA118165, SRP ES010337 and AI0043477 to M.K.; and DK099558 to Y.H.), the Hildyard chair for Mitochondrial and Metabolic Diseases (M.K.), the Japan Society for the Promotion of Science (K.T.), Irma T Hirschl Trust (Y.H.), the FLAGS foundation (N.G.) and the Uehara Memorial Foundation (S.N.).

AUTHOR CONTRIBUTIONS

K.R., M.Ka., M.H., Y.B.-N. and E.P. conceived of the study; S.F., D.Y. and I.S. designed and carried out most experiments and data analysis; K.T., A.W., K.U., N.G., S.N., G.G., M.E.S., M.Ko., H.K., M.B. and O.P. carried out additional experiments, contributed samples and performed data analysis; J.L.B. and K.R. supplied reagents; and S.F., D.Y., I.S., Y.H., M.Ka., M.H., Y.B.-N. and E.P. wrote the manuscript.

COMPETING FINANCIAL INTERESTS

The authors declare competing financial interests: details are available in the [online version of the paper](#).

Reprints and permissions information is available online at <http://www.nature.com/reprints/index.html>.

- Coppola, D. *et al.* Unique ectopic lymph node-like structures present in human primary colorectal carcinoma are identified by immune gene array profiling. *Am. J. Pathol.* **179**, 37–45 (2011).
- Pitzalis, C., Jones, G.W., Bombardieri, M. & Jones, S.A. Ectopic lymphoid-like structures in infection, cancer and autoimmunity. *Nat. Rev. Immunol.* **14**, 447–462 (2014).
- Di Caro, G. *et al.* Occurrence of tertiary lymphoid tissue is associated with T-cell infiltration and predicts better prognosis in early-stage colorectal cancers. *Clin. Cancer Res.* **20**, 2147–2158 (2014).
- Dieu-Nosjean, M.C. *et al.* Long-term survival for patients with non-small-cell lung cancer with intratumoral lymphoid structures. *Journal of clinical oncol.* **2008**, 26(27) 4410–4417.
- Gu-Trantien, C. *et al.* CD4(+) follicular helper T cell infiltration predicts breast cancer survival. *J. Clin. Invest.* **123**, 2873–2892 (2013).
- Messina, J.L. *et al.* 12-Chemokine gene signature identifies lymph node-like structures in melanoma: potential for patient selection for immunotherapy? *Sci. Rep.* **2**, 765 (2012).
- Di Caro, G. & Marchesi, F. Tertiary lymphoid tissue: A gateway for T cells in the tumor microenvironment. *OncolImmunology* **3**, e28850 (2014).
- Torrecilla, S. & Llovet, J.M. New molecular therapies for hepatocellular carcinoma. *Clin. Res. Hepatol. Gastroenterol.* **39**, S80–S85 (2015).
- El-Serag, H.B. Hepatocellular carcinoma. *N. Engl. J. Med.* **365**, 1118–1127 (2011).
- Umemura, A. *et al.* Liver damage, inflammation, and enhanced tumorigenesis after persistent mTORC1 inhibition. *Cell Metab.* **20**, 133–144 (2014).
- Scheuer, P.J., Ashrafzadeh, P., Sherlock, S., Brown, D. & Dusheiko, G.M. The pathology of hepatitis C. *Hepatology* **15**, 567–571 (1992).
- Gerber, M.A. Histopathology of HCV infection. *Clin. Liver Dis.* **1**, 529–541 (1997).
- Hoshida, Y. *et al.* Gene expression in fixed tissues and outcome in hepatocellular carcinoma. *N. Engl. J. Med.* **359**, 1995–2004 (2008).
- Murakami, J. *et al.* Functional B-cell response in intrahepatic lymphoid follicles in chronic hepatitis C. *Hepatology* **30**, 143–150 (1999).
- Hoshida, Y., Villanueva, A. & Llovet, J.M. Molecular profiling to predict hepatocellular carcinoma outcome. *Expert Rev. Gastroenterol. Hepatol.* **3**, 101–103 (2009).
- Drayton, D.L., Liao, S., Mounzer, R.H. & Ruddle, N.H. Lymphoid organ development: from ontogeny to neogenesis. *Nat. Immunol.* **7**, 344–353 (2006).
- Sasaki, Y. *et al.* Canonical NF- κ B activity, dispensable for B cell development, replaces BAFF-receptor signals and promotes B cell proliferation upon activation. *Immunity* **24**, 729–739 (2006).
- Postic, C. & Magnuson, M.A. DNA excision in liver by an albumin-Cre transgene occurs progressively with age. *Genesis* **26**, 149–150 (2000).
- Pikarsky, E. *et al.* NF- κ B functions as a tumour promoter in inflammation-associated cancer. *Nature* **431**, 461–466 (2004).
- Cairo, S. *et al.* Hepatic stem-like phenotype and interplay of Wnt/ β -catenin and Myc signaling in aggressive childhood liver cancer. *Cancer Cell* **14**, 471–484 (2008).
- He, G. *et al.* Identification of liver cancer progenitors whose malignant progression depends on autocrine IL-6 signaling. *Cell* **155**, 384–396 (2013).
- Wada, Y., Nakashima, O., Kutami, R., Yamamoto, O. & Kojiro, M. Clinicopathological study on hepatocellular carcinoma with lymphocytic infiltration. *Hepatology* **27**, 407–414 (1998).
- Schneider, C. *et al.* Adaptive immunity suppresses formation and progression of diethylnitrosamine-induced liver cancer. *Gut* **61**, 1733–1743 (2012).
- Okin, D. & Medzhitov, R. Evolution of inflammatory diseases. *Curr. Biol.* **22**, R733–R740 (2012).
- Karin, M., Lawrence, T. & Nizet, V. Innate immunity gone awry: linking microbial infections to chronic inflammation and cancer. *Cell* **124**, 823–835 (2006).
- Haybaeck, J. *et al.* A lymphotoxin-driven pathway to hepatocellular carcinoma. *Cancer Cell* **16**, 295–308 (2009).
- Wolf, M.J., Selezniuk, G.M. & Heikenwalder, M. Lymphotoxin's link to carcinogenesis: friend or foe? from lymphoid neogenesis to hepatocellular carcinoma and prostate cancer. *Adv. Exp. Med. Biol.* **691**, 231–249 (2011).
- Tumanov, A.V. *et al.* T cell-derived lymphotoxin regulates liver regeneration. *Gastroenterology* **136**, 694–704 (2009).
- Drutskaya, M.S., Efimov, G.A., Kruglov, A.A., Kuprash, D.V. & Nedospasov, S.A. Tumor necrosis factor, lymphotoxin and cancer. *IUBMB Life* **62**, 283–289 (2010).
- Bauer, J. *et al.* Lymphotoxin, NF- κ B, and cancer: the dark side of cytokines. *Dig. Dis.* **30**, 453–468 (2012).
- Yun, C. *et al.* NF- κ B activation by hepatitis B virus X (HBx) protein shifts the cellular fate toward survival. *Cancer Lett.* **184**, 97–104 (2002).
- Yu, G.Y. *et al.* Hepatic expression of HCV RNA-dependent RNA polymerase triggers innate immune signaling and cytokine production. *Mol. Cell* **48**, 313–321 (2012).
- Arzumanyan, A., Reis, H.M. & Feitelson, M.A. Pathogenic mechanisms in HBV- and HCV-associated hepatocellular carcinoma. *Nat. Rev. Cancer* **13**, 123–135 (2013).
- Mosnier, J.F. *et al.* The intraportal lymphoid nodule and its environment in chronic active hepatitis C: an immunohistochemical study. *Hepatology* **17**, 366–371 (1993).
- Qi, H., Kastenmuller, W. & Germain, R.N. Spatiotemporal basis of innate and adaptive immunity in secondary lymphoid tissue. *Annu. Rev. Cell Dev. Biol.* **30**, 141–167 (2014).
- Iwasaki, A. & Medzhitov, R. Regulation of adaptive immunity by the innate immune system. *Science* **327**, 291–295 (2010).
- Verna, L., Whysner, J. & Williams, G.M. N-nitrosodiethylamine mechanistic data and risk assessment: bioactivation, DNA-adduct formation, mutagenicity, and tumor initiation. *Pharmacol. Ther.* **71**, 57–81 (1996).
- Yau, T.O. *et al.* Hepatocyte-specific activation of NF- κ B does not aggravate chemical hepatocarcinogenesis in transgenic mice. *J. Pathol.* **217**, 353–361 (2009).
- Subramanian, A. *et al.* Gene set enrichment analysis: a knowledge-based approach for interpreting genome-wide expression profiles. *Proc. Natl. Acad. Sci. USA* **102**, 15545–15550 (2005).
- Hoshida, Y. Nearest template prediction: a single-sample-based flexible class prediction with confidence assessment. *PLoS ONE* **5**, e15543 (2010).
- Bruix, J. & Sherman, M. American Association for the Study of Liver D. Management of hepatocellular carcinoma: an update. *Hepatology* **53**, 1020–1022 (2011).
- Tian, B., Nowak, D.E., Jamaluddin, M., Wang, S. & Brasier, A.R. Identification of direct genomic targets downstream of the nuclear factor- κ B transcription factor mediating tumor necrosis factor signaling. *J. Biol. Chem.* **280**, 17435–17448 (2005).
- Hinata, K., Gervin, A.M., Jennifer Zhang, Y. & Khavari, P.A. Divergent gene regulation and growth effects by NF- κ B in epithelial and mesenchymal cells of human skin. *Oncogene* **22**, 1955–1964 (2003).

ONLINE METHODS

Prognostic evaluation of histological ELSs, ELS gene signature, and NF- κ B activation in liver tissues from curatively treated patients with HCC. The prognostic association of the ELS gene signature was evaluated in genome-wide transcriptome profiles of cirrhotic liver tissues from 82 surgically treated patients with HCC monitored for up to 15.6 years (median, 7.8 years), reported before (GEO accession code, [GSE10140](#)) (ref. 15). For each patient in the cohort, induction of the ELS gene signature was determined by Kolmogorov-Smirnov statistic-based gene set-enrichment assessment³⁹ implemented in a custom analysis code written in R statistical language. Significance of the signature gene induction was determined as a prediction confidence *P* value (significance threshold, *P* < 0.05) based on null distribution of the statistic generated by random permutation of the samples (*n* = 1,000). Prognostic association of the ELS gene signature was assessed by Kaplan-Meier curves, log-rank test, and multivariable Cox regression modeling adjusted for the 186-gene prognostic-HCC-risk signature reported before and clinical prognostic staging (American Association for Study of Liver Diseases staging system⁴¹). No clinical variables were associated with these clinical outcomes.

Correlation between presence of ELSs and NF- κ B activation was determined by modulation of three experimentally defined NF- κ B target gene signatures in HeLa cells⁴² and primary human fibroblasts and keratinocytes⁴³ and was evaluated in the same transcriptome data set of 82 patients with HCC. Histological ELS features were determined in 66 of the 82 patients with H&E-stained slides as described¹⁴: vague follicular aggregation; definite round-shaped cluster of small lymphocytes without germinal center; and follicles with definite germinal centers composed of large lymphocytes with clear cytoplasm. Each section was observed independently by two reviewers blinded to patient data. A consensus score was reached on a multi-head microscope in cases of discordance. Presence of histological ELS was defined as presence of any of the histological ELS features in $\geq 50\%$ of portal areas for each patient.

Human liver tissue. Human liver biopsy specimens were obtained from the archives of the Institute of Surgical Pathology, University Hospital Zurich, and patients were kept anonymous. The study protocol was approved by the ethical committee of the GesundheitSEMirektion Kanton Zurich (StV 26-2005 and KEK-ZH-Nr. 2013-0382) and was in accordance with the Helsinki declaration guidelines. Additional surgically resected human liver tissues (with identifying information removed) were obtained via Mount Sinai Biorepository (IRB approval HS10-00135).

Mice, HCC induction and anti-Thy-1.2 and LT β R-Ig treatment. All animal experiments were performed in accordance with the guidelines of the Hebrew University, the University of California, San Diego, and the US National Institutes of Health for the use of animals for research. ROSA26-LSL-IKK β (EE) mice (with expression of constitutively active IKK β fused to a Flag tag)¹⁷ were bred with Alb-cre mice¹⁸ (003574; Jackson Laboratory) to generate IKK β (EE)^{Hep} mice. Alb-cre mice served as controls for IKK β (EE)^{Hep} mice. Alb-IKK β (EE) mice were generated at the transgenic mouse facility at the University of California, San Diego, as follows: cDNA encoding hemagglutinin-tagged IKK β (EE)⁴⁴ was amplified by PCR and then inserted into a plasmid containing 2.3-kilobase gene enhancer-promoter encoding mouse albumin, the second intron of the gene encoding rabbit β -globin, the polyadenylation signal of the gene encoding rabbit β -globin and SV40 early gene polyadenylation signal (provided by K. Kohno, Nara Institute of Science and Technology, Nara, Japan)⁴⁵. The expression cassette was excised and purified and then injected into fertilized C57BL/6 oocytes to generate founder mice, three of which transmitted the IKK β (EE) transgene. *Rag1*^{-/-} mice (002216) were from Jackson Laboratory, and *Mdr2*-deficient mice have been described¹⁹. All mice were of a pure C57BL/6 genetic background and were bred and maintained in specific pathogen-free conditions. Only male mice were used. Animals were sacrificed by a lethal dose of anesthesia and underwent perfusion through the left ventricle with heparinized PBS, followed by buffered formalin.

For hepatocarcinogenesis, mice given intraperitoneal injection of DEN (Sigma) at a dose of 10 mg per kg body weight at 15 d of age. Mice were observed for development of tumors at 9 months of age. For inhibition of LT β R signaling, a fusion protein of mouse LT β R and IgG1 (LT β R-Ig; Biogen Idec), was used. Mice were given intraperitoneal injection on a weekly basis

with 100 μ g of LT β R-Ig or control mouse IgG1 (MOPC21; Biogen Idec) for 10 consecutive weeks, starting either at 3 weeks of age ('early'; 3–12 weeks of age), 13 weeks ('intermediate'; 13–22 weeks of age) or 23 weeks ('late'; 23–32 weeks of age). Mice were sacrificed at 33 weeks of age for evaluation of HCC development (Supplementary Fig. 8a).

For treatment with anti-Thy-1.2, mice were given intraperitoneal injection of anti-Thy-1.2 (BE0066; BioXCell), or rat IgG2b isotype-matched control antibody (LTF-2; BE0090; BioXCell) as a control, every 2 d for 12 weeks. Mice were sacrificed at the age of 6.5 months.

Myc-Trp53^{-/-} liver tumors were provided by M.-A. Buendia (Institut Pasteur, France). Mice with transgenic expression of woodchuck hepatitis virus (WHV)/*Myc* were mated with p53-deficient mice to generate mice heterozygous for both the p53 mutation and the *Myc* transgene. The WHV/*Myc* p53^{+/ Δ} mice spontaneously developed HCC, which frequently acquired a deletion of the remaining allele encoding p53. HCCs were further genotyped. *Myc-Trp53*^{-/-} HCCs were used as reference for a highly proliferative liver cancer in the 16-gene array analysis.

Concentrations of alanine transaminase and aspartate aminotransferase in serum were determined with the Reflotron Plus analysis system (Roche).

Examination of H&E-stained mouse sections was performed by three expert liver pathologists (A.W., O.P. & E.P.).

Immunohistochemistry, immunofluorescence and three-dimensional reconstruction. Antibodies used were as follows: anti-A6 (provided by V. Factor and S. Thorgeirsson, US National Institutes of Health); anti-B220 (RA3-6B2; BioLegend), anti-CD3 (CD3-12 (Serotec) or RBK024 (ZYTOMED)), anti-GFP (A-11122; Invitrogen), anti-F4/80 (CI:A3-1; Serotec), anti-Ly-6G (551459; BD Pharmingen), anti-FDC-M1 (FDC-M1; BD Pharmingen), antibody to glutamine synthetase (ab16802; Abcam), anti-GP73/GOLPH2 (sc-48011; Santa Cruz), anti-Foxp3 (FJK-16s; eBioscience), anti-Ki67 (SP6; Thermo Scientific), anti-CDC47 (MCM7) (sc-56324; Santa Cruz), anti-RelA (p65) (RB-1638; NeoMarkers), anti-CD44 (IM7; eBioscience), anti-CD44 (V6) (9A4; eBioscience), Sox9 (sc-20095; Santa Cruz), anti-CK19 (hybridoma TROMA-III; deposited in Developmental Studies Hybridoma Bank by K. Rolf), antibody to collagen IV (CL50451AP; Cedarlane Laboratories), anti-E-cadherin (36/E-cadherin; BD) and antibody to cleaved caspase-3 (9661; Cell Signaling). Antigen retrieval for B220, GFP, Ki67, CDC47, E-cadherin, RelA, Sox9, CK19 and cleaved caspase-3 was performed in 25 mM citrate buffer, pH 6.0, and antigen retrieval for GP73, Ly-6G, glutamine synthetase, collagen IV, Foxp3, CD44, CD44(V6) and CD3 was performed in EDTA buffer pH 8.0 (Invitrogen); all were done by heating of samples to 125 °C for 3 min in a decloaking chamber (Biocare Medical). Antigen retrieval for A6 and F4/80 was performed by incubation with 1 mg/ml Pronase XXIV (Sigma). Immunofluorescence was performed on formalin-fixed and paraffin-embedded sections. Fluorophore-conjugated secondary antibody used were as follows: indocarbocyanine (Cy5)-conjugated donkey anti-mouse (715-175-151; Jackson ImmunoResearch), indocarbocyanine (Cy3)-conjugated donkey anti-rat (712-165-153; Jackson ImmunoResearch) and Alexa Fluor 488-conjugated donkey anti-goat (A-11055; Life Technologies). Hoechst 33342 stain (Invitrogen) was used as a marker of nuclei.

Antibodies used for human sections were as follows: anti-CD3 (103A; Cell Marque), anti-CD15 (CM029; Biocare Medical), anti-CD20 (120R; Cell Marque), anti-CD23 (1B12; Novacastra Labs), anti-CD68 (KP1; Invitrogen), anti-Foxp3 (236A/E7; eBioscience), anti-HSP70 (sc-24; Santa Cruz) and anti-LT β (B27.B2; Biogen). Immunohistochemical staining of human sections was performed with the BenchMark XT system (Ventana) with Cell Conditioning 1 solution (Ventana) for pretreatment, except for Foxp3, which was stained manually with EDTA buffer, pH 8.0 (Invitrogen), for retrieval.

For quantification, stained slides were counted either manually by counting of positive cells per ten high-power fields or through the use of an Ariol SL-50 automated scanning microscope and image-analysis system (Applied Imaging). The frequency of positive cells was assessed with the appropriate module of the Ariol SL-50. For each sample, the percentage of positive cells or the intensity of the staining was determined in ten arbitrarily chosen fields. Three-dimensional reconstruction of ELSs in the liver was done with μ Core software (microDimensions) with a Mirax Midi Slide Scanner (Carl Zeiss microImaging) as described⁴⁶.

Immunoblot analysis and electrophoretic mobility-shift assay. Antibodies used for immunoblot analysis were as follows: anti-actin (AC-40; Sigma), anti-FLAG (M2; Sigma), anti-p100/p52 (4882; Cell Signaling), anti-RelB (06-1105; Milipore) and anti-tubulin (DM-1A; Sigma). For the preparation of whole-cell lysates, tissues were lysed by mechanical grinding in RIPA buffer (50 mM Tris-HCl, pH 7.4, 150 mM NaCl, 1 mM EDTA, 1% NP-40 and 0.25% sodium deoxycholate) containing a 1× mixture of protease inhibitors (Sigma), 10 mM Na₃VO₄, 10 mM Na₄P₂O₇ and 50 mM NaF. Total cell lysates were separated by SDS-PAGE and were assessed by immunoblot analysis by sequential probing with the appropriate primary and the appropriate horseradish peroxidase (HRP)-conjugated antibody to IgG (rabbit (711-035-152) or mouse (115-035-003), both from Jackson ImmunoResearch). Immunoreactive bands were detected with ECL detection reagent (Pierce).

For electrophoretic mobility-shift assay, IRDye 700-labeled oligonucleotide (LI-COR Biosciences) corresponding to the NF- κ B-specific consensus sequence was used. The binding reaction was performed with an Odyssey Infrared electro-mobility shift assay kit (LI-COR Biosciences) according to the manufacturer's protocol. Nuclear proteins were isolated from freshly isolated liver tissue with a Cayman Nuclear Extraction Kit (Cayman Chemical Company), and total protein concentrations were determined with a BCA Protein Assay Kit (Thermo Scientific). 20 ng of total nuclear protein was mixed with the labeled NF- κ B oligonucleotide and was left to bind for 30 min in the dark. Protein-DNA complexes were resolved by electrophoresis through a 4% polyacrylamide Tris-borate-EDTA gel in the dark. Quantitative data were obtained by computerized densitometry and TINA software (version 2.07d; Raytest).

RNA *in situ* hybridization. RNA *in situ* hybridization was performed with an RNAscope 2.0 kit (Advanced Cell Diagnostics) according to the manufacturer's instructions. Formalin-fixed and paraffin-embedded sections 4 μ m in thickness were deparaffinized in xylene and then were pretreated to allow access of probe to target RNA. LT β -specific probe pairs (Advanced Cell Diagnostics) were hybridized to the target RNA for 2 h at 40 °C in a moist hybridization oven. The signal was amplified with alkaline phosphatase-conjugated labeled probes, followed by colorimetric detection with Fast Red as substrate. LT β mRNA was visualized by standard bright-field microscopy.

Array-based CGH. Agilent oligonucleotide array-based CGH for analysis of genomic DNA in formalin-fixed and paraffin-embedded samples (Mouse Genome CGH Microarray 4x44K) was performed on genomic DNA extracted from formalin-fixed and paraffin-embedded liver tissues according to the protocol provided by Agilent Technologies. 500 ng of genomic DNA from the liver was labeled differentially with Cy3-dCTP (HCC) and Cy5-dCTP (liver tissue from C57BL/6 mice) by random-primed labeling (CGH labeling kit for oligo array; Enzo Life Sciences). Genomic DNA from the liver of C57BL/6 mice was pooled and used as reference DNA. After the array slides were scanned, spot fluorescence intensities were extracted with Feature Extraction Software (Agilent Technologies), and the raw data text files were used for further analysis. The data were imported into the R statistical platform (<http://www.R-project.org/>) and data-quality outliers (such as statistical population outliers or spots with foreground/background ratios of less than 3) were filtered out through the use of quality flags as implemented in the Feature Extraction software. The log₂ ratios of each sample were collated into one matrix and were preprocessed and analyzed as follows, with functions from the Bioconductor R package CGHcall⁴⁷. Missing values were replaced with the values from neighboring probes by an imputation algorithm, whereas probes with missing values in more than 30% of samples were excluded from the data set. The remaining data were median-normalized, followed by breakpoint detection with a segmentation algorithm⁴⁸, and the copy-number status (loss, normal and gain) of each segment was determined with the CGHcall function⁴⁷. The copy-number calls of the single probes were transformed into copy-number regions with the CGH regions package⁴⁹ and were plotted for each chromosome according to physical position.

Proliferation and differentiation analysis. Clusters (Fig. 3e) were determined by an unsupervised algorithm and were designated A and B, with the

latter further subdivided into B1 and B2. DEN-induced HCCs from wild-type mice were more similar to wild-type liver parenchyma than to IKK β (EE)^{Hep} HCCs, most of which were in cluster B, together with the aggressive HCCs of *Myc-Trp53*^{-/-} mice. Primer sequences for the 16-gene HCC proliferation and differentiation signature are in **Supplementary Table 7**.

Fluorescence-activated cell sorting. ELSs from IKK β (EE)^{Hep} livers were dissected under a binocular microscope and were digested for 30 min at 37 °C with gentle agitation in 500 μ l digestion buffer (HBSS with 0.2 mg/ml collagenase IV and 0.1 mg/ml DNase I). The cells were strained through 40- μ m filters by being washed with cold DMEM and were centrifuged for 15 min, then red blood cells were lysed for 10 min at 25° with erythrocytes lysis buffer; samples were washed again and then resuspended in 0.5 ml DMEM and kept on ice for a few hours until staining. Viability of isolated cells of the immune system was around 85%, as determined by Trypan blue staining. Cells were resuspended and stained in PBS supplemented with 1% FCS and 1mM EDTA. Samples were stained and then analyzed by flow cytometry with Gallios and Kaluza software (Beckman Coulter), or by fluorescence-activated cell sorting. Antibodies used for flow cytometry were as follows: anti-CD4 (RM-4.5; 100536; BioLegend), anti-CD8 (53-6.7; 65-0081 and 75-008; Tonbo), anti-F4/80 (BM8; 123127; BioLegend), anti-CD11b (M1/70; 101224; BioLegend), anti-MHC class II (KH74; 115303; BioLegend), anti-CD45.2 (104; 109807; BioLegend), anti-NK1.1 (PK136; 12-5941-83; eBioscience), anti-TCR β (H57-597; 35-5961; Tonbo), anti-CD44 (IM7; 103127; BioLegend), anti-CD62L (MEL-14; 104417; BioLegend) and anti-B220 (553090; BD Pharmingen).

Quantitative PCR analysis. Total RNA was extracted with Trizol (Invitrogen) and was reverse-transcribed with a high-capacity cDNA reverse-transcription kit (Applied Biosystems); quantitative PCR was run in triplicate in 384-well plates with SYBR Green (Invitrogen) and a 7900HT Fast Real-Time PCR System (Applied Biosystems) (primer sequences, **Supplementary Tables 3, 6 and 7**). Results were analyzed with Dataassist 2.0 software or qBase software, v1.3.5 (change in expression and *P* values, **Supplementary Tables 2, 4 and 5**). The genes encoding HPRT and PPIA were used as reference genes for human and mouse analyses.

Digital PCR analysis. Genomic DNA was extracted from fresh frozen tissue with DNeasy (69504; QIAGEN) and from formalin-fixed and paraffin-embedded tissue with a QIAamp DNA Micro Kit (56304; QIAGEN) and was used for digital PCR analysis with the following TAQM probes: *Rgs2* (AB-4400291; Applied Biosystems) and *Tert* (AB-4458368; Applied Biosystems). High-throughput droplet digital PCR for quantification of DNA copies was done as described⁵⁰.

Statistical analysis. Statistical significance (*P* < 0.05) was determined by a two-tailed Student's *t*-test, two-tailed χ^2 test or Fisher's exact test. For correlation analysis of mRNA expression, a Spearman or Pearson correlation test at a *P* value of <0.05 was used. Data were processed with Microsoft Excel or GraphPad Prism 6.0 software.

- Delhase, M., Hayakawa, M., Chen, Y. & Karin, M. Positive and negative regulation of I κ B kinase activity through IKK β subunit phosphorylation. *Science* **284**, 309–313 (1999).
- Saito, M. *et al.* Diphtheria toxin receptor-mediated conditional and targeted cell ablation in transgenic mice. *Nat. Biotechnol.* **19**, 746–750 (2001).
- Huang, L.R. *et al.* Intrahepatic myeloid-cell aggregates enable local proliferation of CD8⁺ T cells and successful immunotherapy against chronic viral liver infection. *Nat. Immunol.* **14**, 574–583 (2013).
- van de Wiel, M.A. *et al.* CGHcall: calling aberrations for array CGH tumor profiles. *Bioinformatics* **23**, 892–894 (2007).
- Venkatraman, E.S. & Olshen, A.B. A faster circular binary segmentation algorithm for the analysis of array CGH data. *Bioinformatics* **23**, 657–663 (2007).
- van de Wiel, M.A. & Wieringen, W.N. CGHregions: dimension reduction for array CGH data with minimal information loss. *Cancer Inform.* **3**, 55–63 (2007).
- Hindson, B.J. *et al.* High-throughput droplet digital PCR system for absolute quantitation of DNA copy number. *Anal. Chem.* **83**, 8604–8610 (2011).